Sensors & Actuators: B. Chemical 377 (2023) 133041

Contents lists available at ScienceDirect

Sensors and Actuators: B. Chemical

journal homepage: www.elsevier.com/locate/snb

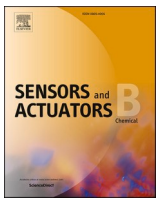

Real-time monitoring of CO2 gas using inverse opal photonic gel containing Poly(2-(dimethylamino)ethylmethacrylate

Nam Yeon Heo [a,1], Shin Geun Park [a,1], Donghoon Kim [a,1], Hyunjung Lee [b], Wonmok Lee [a,*]

[a] Department of Chemistry, Sejong University, 209 Neungdong-ro, Gwangjin-gu, Seoul 05006, South Korea
[b] School of Advanced Materials Engineering, Kookmin University, 77 Jeongneung-ro, Seongbuk-gu, Seoul 02707, South Korea

ARTICLE INFO

Keywords:
CO_2 sensor
Inverse opal photonic gel
Real-time monitoring
Structural color

ABSTRACT

With the rapid progression of global climate changes and air pollution in recent years, there has been growing interest in the sensing and monitoring of CO_2 gas. In the present study, an inverse opal photonic gel (IOPG) colorimetric sensor is demonstrated that is capable of real-time monitoring of CO_2 gas in an open system without the necessity of a power supply. The IOPGs are fabricated via the opal-templated photo-polymerization of monomer mixtures of hydroxyethyl methacrylate and 2-(dimethylamino)ethyl methacrylate (DMAEMA) or 2-(dimethylamino)propyl methacrylamide (DMAPMAm), followed by template removal. When the IOPG sensor is immersed in water with a steady flow of mixed CO_2/N_2 gas at various ratios, the CO_2 molecules dissolve in the water and are converted to carbonate anions, which subsequently bind to the amino groups of pDMAEMA to build up osmotic pressure, thus leading to swelling of the IOPG. A comparison of the sensing and recovery capabilities of the two types of IOPG indicates that the pDMAEMA-containing IOPG exhibits a limit of detection below 1.2%, and 2.6 times faster CO_2 desorption kinetics compared to the pDMAPMAm-containing IOPG. The swelling behavior of the CO_2-responsive IOPG is rigorously investigated at various pH values, and temperatures by analyzing the reflectance spectra of the IOPG in the visible wavelength range. The usefulness of the pDMAEMA-IOPG as a real-time CO_2 sensor was confirmed by applying it to various carbonated drinks.

1. Introduction

Gas sensors are of great importance because the monitoring or sensing of a specific gaseous compound is a prerequisite in a number of fields and applications such as the oil industry, mining, wastewater, medical devices, power stations, etc. [1–3] In particular, CO_2 gas sensing has been of significant interest to researchers not only because it is the most important greenhouse gas involved in global warming, but also because the monitoring of CO_2 is critically required in many applications. In a hospital intensive care unit (ICU), for example, the CO_2 level of the patients' exhaled breath should be continuously monitored. [4] Moreover, because CO_2 is an asphyxiant gas in confined spaces with a limited air supply, the monitoring of CO_2 concentration is essential for submarine, aerospace, and mining environments. In addition, the tracking of industrial CO_2 emission during food production or packaging is important. [5].

Many different types of CO_2 gas sensor have been reported, including the very sensitive tool of infrared spectroscopy, although interference from CO gas and water vapor limits a quantitative analysis. [6,7] The electrochemical detection of CO_2 has also been investigated in various ways. For example, Lang et al. reported that the variation in CO_2 pressure when the dissolved CO_2 reacts with oxygen to produce carbonate anions can be measured potentiometrically with limit of detection (LOD) below 0.5 vol%. [8] More recently, solid electrolytes have been found to provide high sensitivities and fast responses for the potentiometric detection of CO_2.[9] Although electrochemical detection of CO_2 gas provides an LOD of 0.4% or lower, all of these CO_2 sensors require an electric power supply for operation, and the powerless detection of CO_2 gas might be demanded in special cases such as the monitoring of food decomposition or fermentation.[10].

Recently, colorimetric photonic gel sensors have been developed, in which the sensing response is provided by the change in reflective color due to the difference in the lattice distances of the imbedded colloidal crystal structure before and after analyte binding. [11–22] While measurement of the Donnan potential (i.e., the potential difference across an interface between two immiscible electrolyte solutions when one ionic

* Corresponding author.
E-mail address: wonmoklee@sejong.ac.kr (W. Lee).
[1] These authors contributed equally to this work

https://doi.org/10.1016/j.snb.2022.133041
Received 11 September 2022; Received in revised form 20 November 2022; Accepted 21 November 2022
Available online 24 November 2022

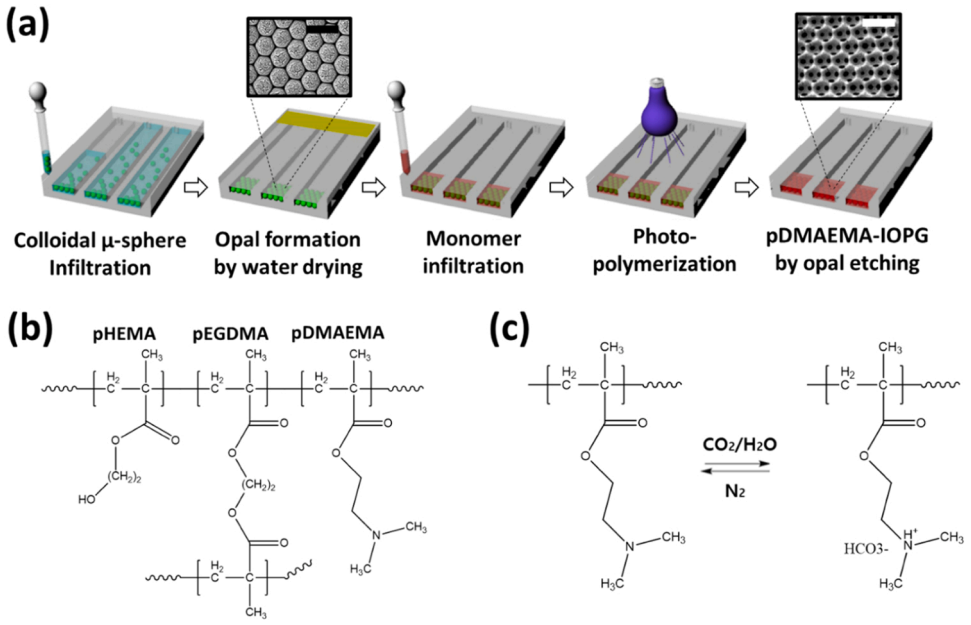

Fig. 1. (a) Schematic diagrams showing the fabrication of the CO_2-responsive inverse opal photonic gel, along with SEM images (scale bar = 500 nm) of the opal template and the IOPG, respectively. (b) The chemical structure of pDMAEMA-IOPG. (c) The intramolecular charge generation of pDMAEMA upon reaction with dissolved CO_2 and H_2O.

solute is unable cross over while other ions are free to cross in both directions) can identify the sensing response [11,12,15–17,20,22], the photonic gel sensor features repeatable color changes which can be recognized by the naked eye, thus making it suitable for continuous analyte monitoring. Moreover, it can be operated without the need for complex instrumentation or an electric power supply. Depending upon the specific fabrication strategy, the photonic gel sensor can be categorized as a polymerized crystalline colloidal array (PCCA) or an inverse opal photonic gel (IOPG). In each case, various sensor applications have been investigated, including the measurement of glucose [11], anion [23], cation [12], volatile organic compound (VOC),[22] and pH,[16, 17] temperature [24–26], and humidity[27]. In particular, the IOPG provides rapid responses owing to its highly porous structure, and its use in colorimetric CO_2 sensing has been reported in a recent publication. [15] In that study, a silica opal templated hydrogel containing dimethylaminopropyl methacrylamide (DMAPAMAm) was fabricated, and DMAPAMAm was found to efficiently bind with dissolved CO_2 in water to generate a change in Donnan potential, and quantitative colorimetric analysis of the CO_2 concentration with LOD below 1.2% in air was successfully demonstrated. However, the analysis was performed in a confined space, where the IOPG sensor changed color in response to dissolved CO_2 gas. The in-situ monitoring of CO_2 concentration requires further study from the practical view point. In another recent investigation, a cellulose particle grafted with 2-(dimethylamino)ethyl methacrylate (DMAEMA) showed a better CO_2 sensing kinetic response and repeatability compared to those of a DMAPMAm-grafted particle.[28].

In the present study, the real-time monitoring of CO_2 concentration in air is investigated by fabricating an efficient CO_2 sensing IOPG containing DMAEMA, and the kinetic response of the IOPG sensor is rigorously investigated.

2. Experimental section

2.1. Materials

For the synthesis of polystyrene (PS) microspheres, styrene (>99%,), potassium persulfate (KPS, 99.99%), and sodium dodecyl sulfate (SDS, >99.8%) were purchased from Sigma Aldrich. Aluminum oxide (Sigma Aldrich) was used for purification of the styrene, and an ion exchange resin (AG501-X8,Bio-Rad) was used for preservation of the PS emulsion in water. Hydrogen peroxide (H_2O_2), isoocatane, ammonia water (NH_4OH; 25–30%), and ethanol were purchased from Duksan, and trichlorooctadecyl silane was purchased from Sigma Aldrich. These were all used without further purification for cleaning the glass substrates. For preparation of the IOPG, 2-hydroxyethyl methacrylate (HEMA, 97%) and ethylene glycol dimethacrylate (EGDMA, 98%) were purchased from Sigma Aldrich, 2,2-dimethoxy-2-phenylacetophenone (Irgacure-651) was obtained from Ciba Specialty Chemicals, 2-(dimethylamino) ethylmethacrylate (DMAEMA, 98.5% and N-(3-dimethylamino)propylmethacrylamide (DMAPMAm, 98.5%) were purchased from TCI; these were used without further purification. For removal of the PS template, chloroform and acetonitrile were purchased from SAMCHUN.

2.2. Synthesis of PS microspheres

The PS microspheres were synthesized by emulsion polymerization. {Kim, 2010 #2360} For the synthesis of PS microsphere with 230 nm diameter, a 500-mL round-bottomed flask was charged with deionized (DI) water (300 mL), and degassed by N_2 bubbling for 30 min. Then, KPS (1.0 g) and SDS (0.085 g) were dissolved in a small aliquot of DI water, and added to the flask. The flask was then heated to 70 °C under an N_2 atmosphere, and styrene monomer (60 mL) was injected after passing through aluminum oxide. The emulsion polymerization reaction was allowed to proceed for 4 h under vigorous mechanical stirring. The as-synthesized PS microsphere emulsion was then filtered through cotton wool and purified by dialysis in a cellulose membrane tube. By changing the amount of SDS from 0.085 to 0.095 g, the PS microsphere with particle diameter of 200 nm was also prepared. Average sizes and standard deviations of PS particles were calculated from a scanning electron microscopy image, and the coefficient of size variations were calculated to be 5% for PS-200%, and 6% for PS-230 respectively, which are small enough for artificial opal templating. (Fig. S1 of the Supporting information).

2.3. Preparation of the opal template

The initial peak wavelength (λ_{peak}) of the sensor can be controlled by the size of the microspheres used for opal templating (Fig. S1). In the

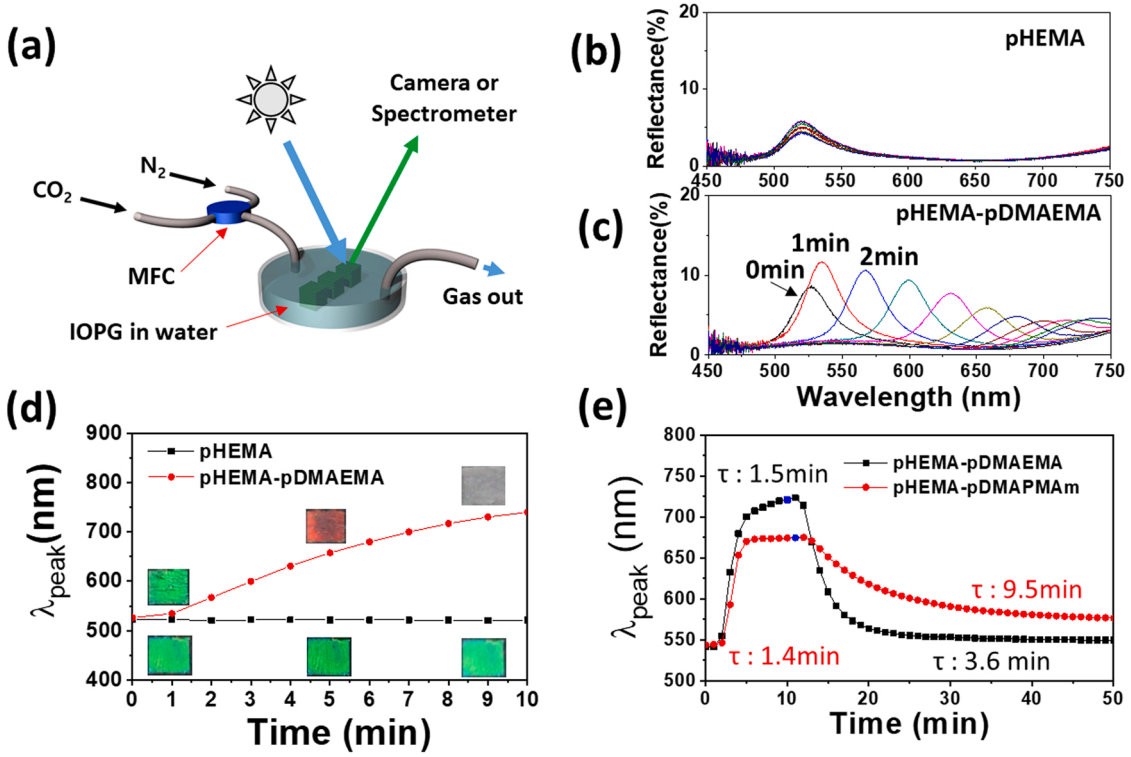

Fig. 2. (a) A schematic diagram of the CO_2 sensing experiment. CO_2 is premixed with N_2 in various ratios before flowing into a cell which contains an IOPG in water, and exit via gas outlet hole. Color change of the IOPG is monitored either by a camera or a fiber-optic spectrometer. (b) The time-dependent reflectance spectra of the pHEMA-IOPG under a CO_2 supply of 25 mL/min. (c) The time-dependent reflectance spectra of the pDMAEMA-IOPG under a CO_2 supply of 25 mL/min. (d) The plots of λ_{peak} vs. time obtained from (b) and (c), with inset optical photographs of the IOPGs obtained at 1, 5, and 9 min, respectively. (e) The plots of λ_{peak} vs. time obtained for the pDMAEMA- and pDMAPMAm-IOPGs under the same CO_2 flow rate (25 mL/min) and concentration. Here, the CO_2 supply was started at 0 min, and was switched to N_2 at 10 min.

present study, PS microspheres with an average diameter of 230 nm were used in most cases. A glass slide was cut in half for use as a bottom substrate and a top slide. Three holes ($\varphi = 2$ mm) were drilled in the top slide for infiltration of the PS emulsion. The top and bottom glass slides were treated with boiling RCA solution (i.e., 1:1:5 NH_4OH:H_2O_2:DI water by volume), then rinsed with DI water. After drying, the top slide was soaked in 0.1 wt% trichlorooctadecylsilane in isooctane for 30 min, and rinsed with ethanol.

As shown in Fig. 1(a), three channels were cut into a 25-μm surlyn film, and this was inserted beween the top and bottom slides so that the three holes in the top slide would be positioned over the three channels. The assembled cell was hot-pressed for 15 s at 70 °C. Using a micro-pipette, a 14-wt% PS aqueous dispersion was infiltrated through the holes, which were then taped over to prevent water evaporation until required. When required, the tape was removed from the holes and water was allowed to evaporate for 4 h; the resulting 25 μm-thick opal films were then annealed overnight at 80 °C.[29] The designation pHEMA-IOPG refers to the IOPG with the copolymeric structure pHEMA-co-pEGDMA, and the designation pDMAEMA-IOPG refers to the IOPG with the copolymeric structure shown in Fig. 1(b), i.e., pHEMA-co-pEGDMA-co-pDMAEMA, which is designed to have a rapid CO_2 response due to a highly porous structure of IOPG as shown in Fig. 1 (a).[20].

2.4. Preparation of the CO_2-responsive IOPG

In a typical preparation, HEMA (0.6 g), EGDM (0.016 g), Irgacure 651 (0.008 g), DI water (0.144 g), and DMAEMA (0.125 g) were mixed in a 20-mL vial. One or two drops of the precursor mixture were then placed on a front inlet of the opal film until they completely infiltrated the interstitial volume of the template film. The precursor-infiltrated opal film was then exposed to UV light (Spectroline) through a neutral density filter (optical density = 3.0, Edmund Optics) for 30 min until the polymerization reaction was complete. The bottom substrate with the polymerized film was then separated from the top slide, and dissolved in chloroform to remove the opal film. The film was then washed with chloroform, acetonitrile, and DI water, and finally stored in DI water.

2.5. The CO_2 sensing experiment

In this experiment, separate mass flow controllers (MFCs, Line Tech.) were used to precisely control the flow of the CO_2 and N_2 gases. After passing through their respective MFCs, the gases were mixed at a 3-way valve, and the mixed gas was introduced through a 19 gauge needle to a sealed glass dish (total volume ~5 mL) containing the CO_2-responsive IOPG immersed in DI water (Fig. 2a). The needle was placed ~3 mm above the water surface. To maintain the total gas pressure inside the dish at atmospheric pressure, an outlet hole was made on the other side of the gas inlet. The gas flow rate was fixed at 50 mL/min, and the CO_2 concentration was varied by controlling the flow rate of each gas. The supplied CO_2 gas dissolves in the water and immediately reacts with water molecule to form H_2CO_3, which subsequently neutralizes the dimethylamino groups in pDMAEMA, as shown in Fig. 1(c). The protonated pDMAEMA hydrogel induces a Donnan potential within the gel, which becomes swollen by the water influx. The sensing response of the IOPG (area = 4 ×7 mm^2) was monitored by measuring the reflectance spectrum of the IOPG using a fiber optic UV–vis spectrometer (AvaSpec-3648, Avantes) connected to an optical microscope (S39A, LEAM solution) with a 20x objective lens.[23] The structures and shapes of the opal template and IOPG were characterized using a field-emission scanning electron microscope (FE-SEM; SU-8010, HITACHI).

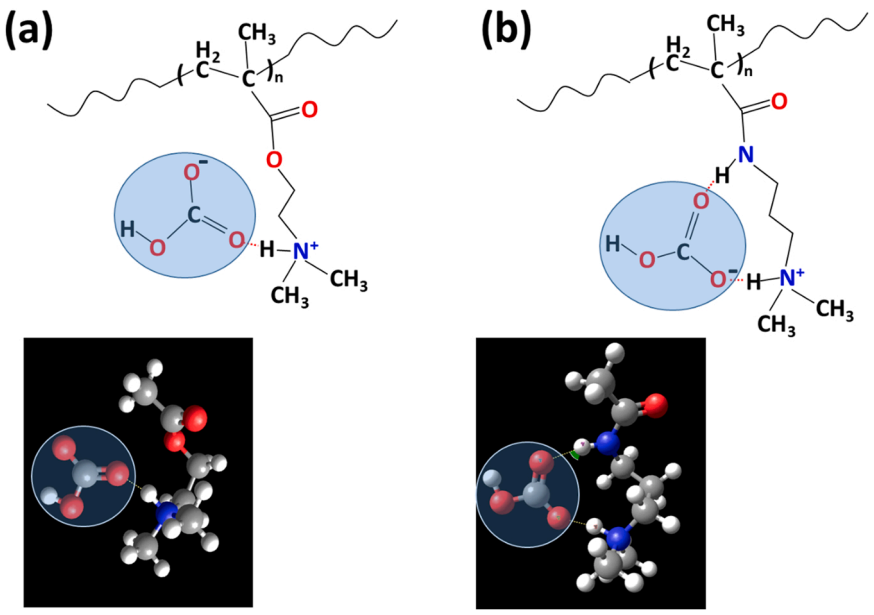

Fig. 3. Schematic drawing of bicarbonate anions bound to dimethylamino groups of (a) pDMAEMA, and (b) pDMAPMAm. Inset figures are the energy-minimized "ball-and-stick" modeled structures of bicarbonate anions (white circle) bound to the analogs of each dimethylamino compound. Oxygen and nitrogen atoms are shown in red and blue balls respectively. Simultaneous H-bonding of bicarbonate with amide N-H of DMAPMAm is evidently shown.

2.6. Molecular simulation

The interactions between bicarbonate anion with pDMAEMA and pDMAPMAm were simulated by using Avogadro™, a free open source molecular editor software (S/W).[30] To simplify the calculation, the analogs of two polymers containing only the substituents of polymer chains were produced, and the energy minimization between each molecular analog and a bicarbonate anion was carried out under auto-optimization setting with MMFF94 force field using steepest descent algorithm.

3. Results and Discussion

CO_2 sensing was carried out using an experimental setup as shown in Fig. 2(a). CO_2 gas is mixed with N_2 gas at MFC, and flows through a cell containing an IOPG sensor or sensor arrays that are immersed in DI water, and leaves the cell via a gas outlet. The highly ordered IO structure of the IOPG enables Bragg diffraction of light of a given wavelength (λ_{peak}) from the (111) layers of the mixed face centered cubic and hexagonal closed packed structure with an effective refractive index (n_{eff}) of an IOPG in water, according to the distance (d) between the pores (λ_{peak}=1.633 x n_{eff} x d).[29] Thus, the CO_2 responses of the two IOPG sensors can be compared by the time-dependent reflectance spectra in Fig. 2(b). Here, the spectrum of the pHEMA-IOPG is unchanged upon exposure to CO_2 gas due to the absence of the amine group. By contrast, the pDMAEMA-IOPG exhibits substantial time-dependent red shifts in the peak reflectance positions (λ_{peak}) upon expossure to CO_2 (Fig. 2(c)). Further, the kinetic responses of the two IOPGs are effectively compared by plotting λ_{peak} vs. time on the same chart in Fig. 2(d), where the inset photographs clearly reveal the color changes of the pDMAEMA-IOPG upon CO_2 exposure. This is the most representative feature of the colorimetric sensor, and enables the intuitive and prompt recognition of the toxic gas. Further, the CO_2 response of the as-fabricated pDMAEMA-IOPG is compared with that of the previously-reported pDMAPMAm-IOPG[15] in Fig. 2(e). Here, the single exponential function fit in the range of interest gives the response time τ

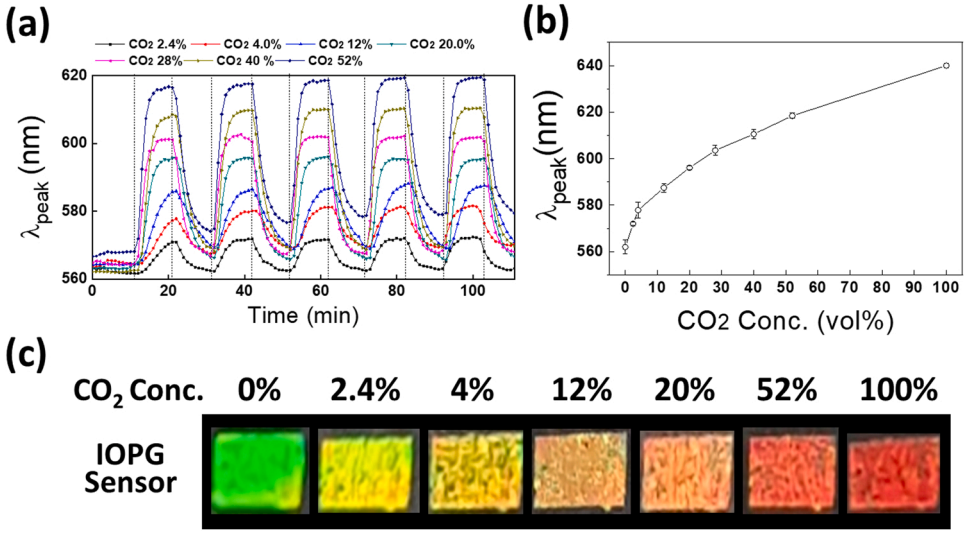

Fig. 4. (a) The reversible response of the pDMAEMA-IOPG under cyclic switching between CO_2 and N_2 at 10-min intervals, where the colored profiles indicate various CO_2 concentrations of 2.4–52% under a fixed total gas flow rate of 25 mL/min. N_2-CO_2 switching time is demonstrated in the graph by dashed line after correction of delay volume. (b) The CO_2 sensitivity of the pDMAEMA-IOPG over the entire range of CO_2 concentrations. (c) The color changes of the pDMAEMA-IOPG at various CO_2 concentrationss.

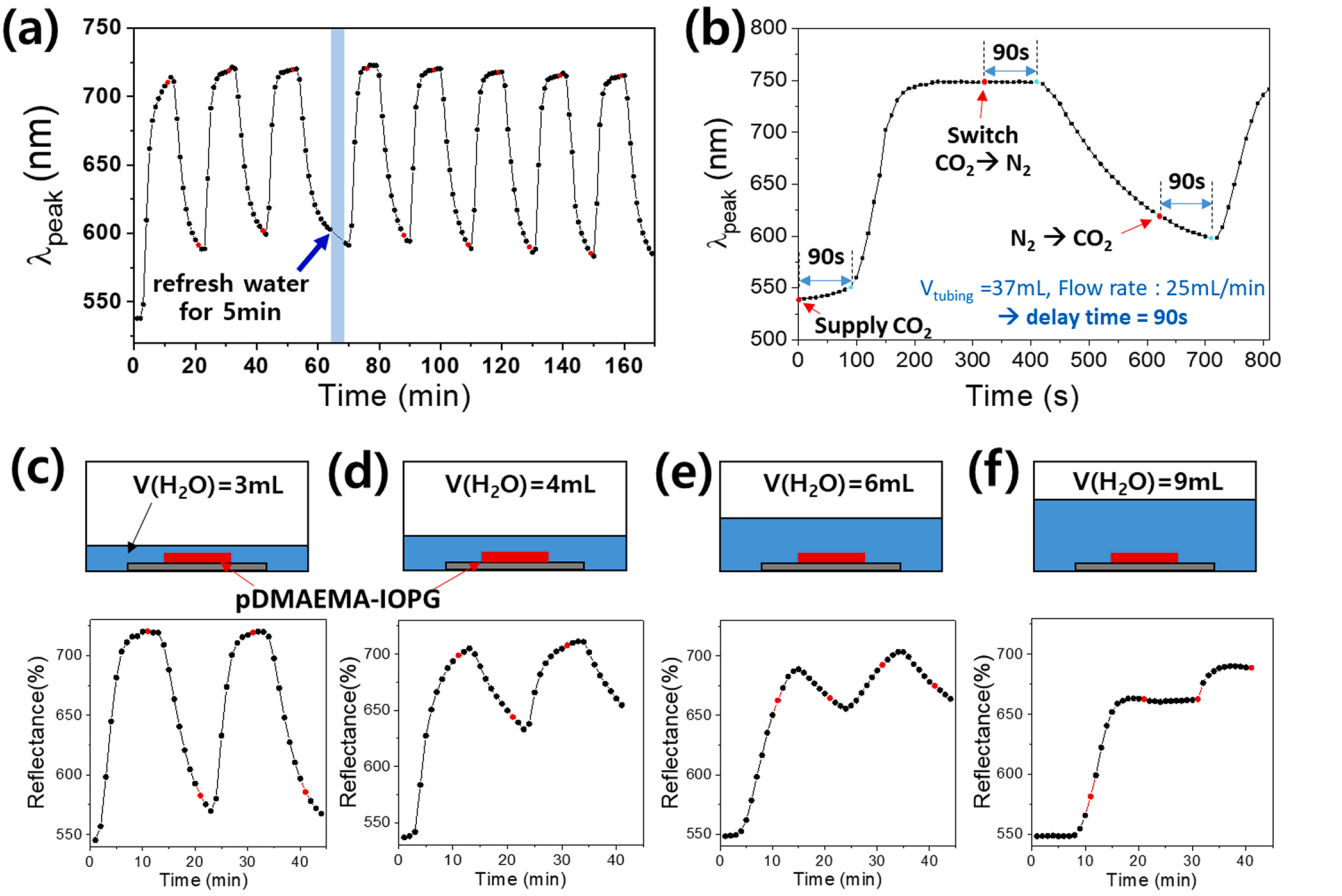

Fig. 5. The real-time sensing responses of the pDMAEMA-IOPG (a) when immersed in 3 mL DI water and subjected to repeated 10-min CO_2/N_2 cycles, with the replacement of ~2.5 mL of DI water at 60 min, (b) at a CO_2/N_2 switching time of 5 min, indicating the anticipated 90-s response delay time, and (c–f) with flow-cell water volumes of (c) 3 mL, (d) 4 mL, (e) 6 mL, and (f) 9 mL, as shown schematically above each response plot.

(Fig. S2). Thus, the pDMAEMA-IOPG exhibits a higher sensitivity (swelling ratio = $\Delta\lambda_{peak}/\lambda_{peak}$) and faster response kinetics (shorter response time, τ) than the pDMAPMAm-IOPG, especially when switching off the CO_2 supply. This can be attributed to the lower pKa of DMAEMA (8.4) compared to that of DMAPMAm (9.2), which provides a stronger thermodynamic driving force related to the Donnan equilibrium.[16,31] Meanwhile, the slower CO_2-removal kinetics of the pDMAPMAm-IOPG compared to the DMAEMA-IOPG may originate from the different molecular structures of the two substituents. Although CO_2-amine reaction in an aqueous system is well known, the binding energy between them can vary depending on different molecular structures of amine.[32] Upon binding with the cationic dimethylamino group in pDMAPMAm, the bicarbonate anion can be hydrogen-bonded to the adjacent amide N–H, which can bring about a retarded desorption.[33,34] By contrast, the DMAEMA does not provide an additional hydrogen bonding interaction with the bicarbonate and, hence, shows a faster response time for desorption. As schematically shown in Fig. 3(a), bicarbonate anion is bound to only dimethylamino group of pDMAEMA, while the simultaneous hydrogen-bonds between a bicarbonate with pDMAPMAm occur as shown in Fig. 3(b). In the schematic drawings shown in Fig. 3(a) and (b), 30% of polymer backbone is pDMAEMA or pDMAPMAm, while 70% is consisted of pHEMA as shown in Fig. 1(b). Through a molecular simulation using Avogadro™, it was confirmed that a bicarbonate shows a double hydrogen-bonded structure with two nitrogens (blue colored ball in each inset figure of Figure3) in an analog of DMAPMAm while a single hydrogen bonded structure occurs between a bicarbonate and DMAEMA analog. The minimum energies of each structure as shown as inset figures in Fig. 3a and b differed by 21% (−935 kJ/mol vs. −770 kJ/mol). The different bonding energetics of the bicarbonate is important because the response time and reproducibility of the CO_2 sensor are critical factors for practical application.

In addition to the molecular aspect of the binding response, both sensors exhibit time delays of about 2 min in their sensing responses due to the void volume, which will be further discussed later in this study. Although the CO_2-sensitivity of the pDMAEMA-IOPG is found to increase as the DMAEMA content is increased (Fig. S3a), the DMAEMA content is fixed at 23 mol.% in the following experiments because this provides the optimum color tunability in the visible wavelength range for CO_2 concentrations of up to 100%.

The reversible response of the pDMAEMA-IOPG under cyclic switching between CO_2 and N_2 at 10-min intervals are shown in Fig. 4 (a), where the colored profiles indicate various CO_2 concentrations of 2.4–52% under a fixed total gas flow rate of 25 mL/min. Here, the pDMAEMA-IOPG shows a λ_{peak} of 562 ± 3 nm under an atmosphere of air and N_2 gas. However, under a flow of 2.4% CO_2, the λ_{peak} is shifted to 572 nm, which corresponds to a $\Delta\lambda_{peak}/\lambda_{peak}$ of 1.8%. In this study, the lowest CO_2 concentration that can be supplied by the MFC was 1.2%. Fig. S3 shows that a red shift ($\Delta\lambda_{peak}$) upon 1.2% CO2 gas is 7 nm while the base line drift can be as large as 2 nm at N_2 flow condition. Taking into account ~1 nm of noise level and ~2 nm λ_{peak} drift of IOPG sensor upon N_2 gas flow, S/N ratio for 1.2% CO_2 sensing is calculated to be larger than 3, and thus the LOD of a given IOPG is expected to be below 1%. As demonstrated in Fig. S3a, LOD of the CO_2 sensor can further be improved by increasing DMAEMA content in pDMAEMA-IOPG fabrication. Exponential function fit showed that the average ascending response time (τ) for the sensor upon 2.4% CO_2 is calculated to be 1.8 min. Upon switching the gas supply from 2.4% CO_2 to N_2, the λ_{peak} is seen to return to its initial value, with a descending τ of 6.8 min. The

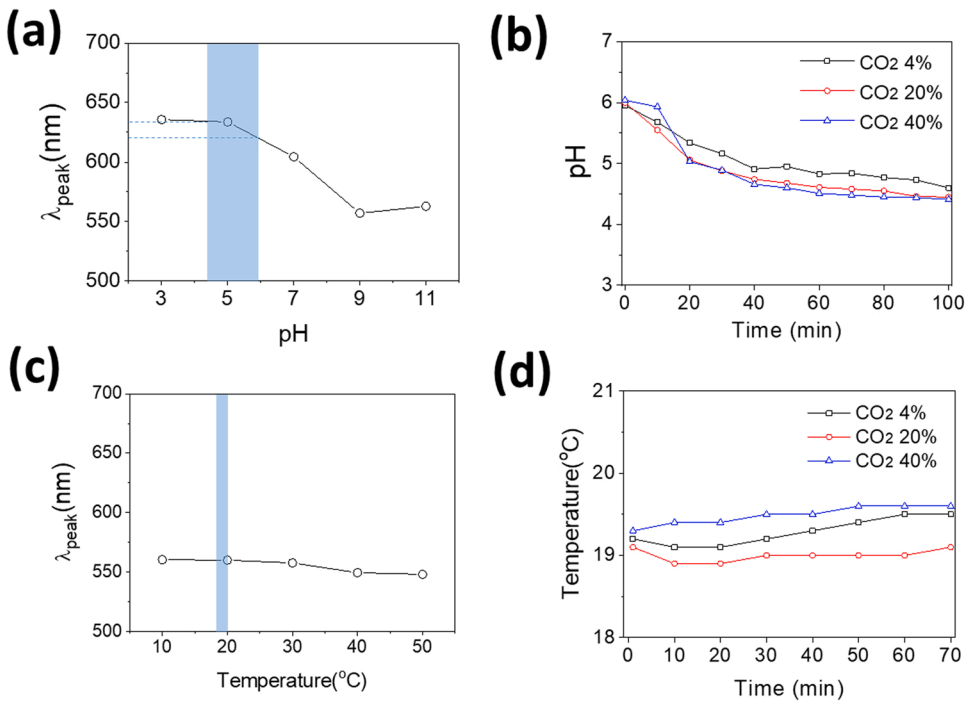

Fig. 6. (a) The pH-driven change in the λ_{peak} of the pDMAEMA-IOPG in 10^{-3} M phosphate buffer solutions at five different pH values, where the blue rectangle indicates the pH value during CO_2 supply. (b) The pH changes of DI water when supplied with various concentrations of CO_2 at a set flow rate of 25 mL/min without physical agitation. (c) The temperature-driven changes in the λ_{peak} of the pDMAEMA-IOPG without CO_2 supply, where the blue rectangle indicates the temperature range during CO_2 sensing. (d) The temperature of the flow cell during CO_2 sensing at various CO_2 concentrations with a fixed flow rate of 25 mL/min.

results of five repeated CO_2 and N_2 switching cycles in Fig. 4(a) demonstrate the outstanding reproducibility of the sensing response. Moreover, this excellent reproducibility is evident at increased CO_2 concentrations of up to 62%, with little change in the ascending and descending response times. These results demonstrate the usefulness of the as-fabricated pDMAEMA-IOPG for real-time CO_2 monitoring.

The graph in Fig. 4(b) indicates a quantitative increase in the λ_{peak} of the pDMAEMA-IOPG with increased CO_2 concentration over the entire concentration range. The reflectance spectra obtained at 30 s intervals at different CO_2 concentration are provided in Fig. S4. Further, the batch-to-batch reproducibility of the pDMAEMA-IOPG is demonstrated by the plots of swelling ratio vs. CO_2 concentration for three individual pDMAEMA-IOPGs in Fig. S5. Moreover, the applicability of the as-fabricated pDMAEMA-IOPG as a practical CO_2 gas sensor is well demonstrated by the clear and reproducible color change in response to CO_2 gas at various concentrations in Fig. 4(c). Here, the pDMAEMA-IOPG exhibits a green color in the absence of CO_2 gas, and a clear color change to yellow, then orange, and then red upon exposure to increasing concentrations CO_2 gas. This change is consistent with the concept of green signalling "safe and sound" (corresponding to very low CO_2 concentrations), and red signalling "danger" at very high CO_2 concentrations. The reproducible color changes of the pDMAEMA-IOPG, and the corresponding λ_{peak} variations, upon exposure to 20% CO_2 are shown in the Supporting movie clips.

The reproducible real-time CO_2 sensing responses of the pDMAEMA-IOPG immersed to various levels and in various volumes of DI water are more rigorously investigated in Fig. 5.

In Fig. 5(a), the pDMAEMA-IOPG is immersed in 3 mL of DI water and subjected to a flow of 40% CO_2 at a rate of 25 mL/min for 10 min, after which the gas is switched to N_2 for 10 min. Under the continuous flow of gas, the water will evaporate and, hence, replacement or refilling will be necessary in order to maintain a constant water level. Therefore, after three such CO_2/N_2 cycles (at t = 60 min), without stopping the N_2 supply, 2.5 mL of the water are drained and replaced by 2.5 mL of fresh DI water (indicated by the arrow in Fig. 5(a)), then another 5 CO_2/N_2 cycles are performed. The λ_{peak} values at the gas switching times are indicated by the red points in the plot. After replacing the water, λ_{peak} is seen to decrease by no more than 15 nm, and the subsequent CO_2 supply results in a well reproducible red shift, thus indicating that water replacement has no visible effect upon the sensor response. In the experimental setup, each gas is delivered through flexible tubing, with ~37 mL of void volume occupied by the tubing between the MFC and the flow cell. Thus, at a gas flow rate of 25 mL/min, about 90 s are required for the target gas to be delivered to the cell upon MFC switching. In other words, the sensor response should be delayed by at least 90 min after gas switching. This is demonstrated in Fig. 5(b), where the reflectance measurements obtained at 10 s intervals are seen to increase approximately 90 s after commencing the supply of 100% CO_2, then decrease 90 s after the supply is switched to N_2, and finally increase 90 s after the flow of CO_2 is repeated. When the flow cell (a petri dish with a diameter of 5 cm and a surface area of 20 cm^2) is charged with 3 mL of DI water, the height of water above the IOPG is ~1 mm, and the addition of 1 mL DI water increases the water level by ~0.5 mm (schematic diagram, Fig. 5(c)). In the absence of forced agitation, the CO_2 gas sensing is further delayed by the increased water level, which affects the diffusion distance of H_2CO_3 to reach the IOPG. The effects of gradually increasing the water level in the flow cell are demonstrated in Fig. 5(c–f), where the response kinetics are seen to be seriously deteriorated at high water levels in the absence of stirring.

In the present study, IOPG is immersed in DI water, and there is an inevitable pH changes upon CO_2 dissolution in water. Despite such pH change, the sensor response was maximized in DI water. If a buffer solution is used to minimize pH change during in-situ CO_2 monitoring, the sensitivity of pDMAEMA-IOPG substantially decreased due to a salt-driven swelling effect.

The pH-dependence of the reflectance spectrum of the pDMAEMA-IOPG is indicated in Fig. S7a, and the λ_{peak} obtained from each spectrum is plotted against pH for 5 different buffer solutions in Fig. 6(a). Here, λ_{peak} is seen to change significantly around pH 7–9, which can be attributed to the pK_b of DMAEMA (8.4), but remains no more than 15 nm (the blue dashed lines, Fig. 6(a)) within the pH region of interest (the blue rectangle, Fig. 6(a)).

When CO_2 is supplied to the flow cell where an IOPG is immersed in DI water, there is an unavoidable pH change due to conversion of the dissolved CO_2 to carbonic acid in accordance with the formula:

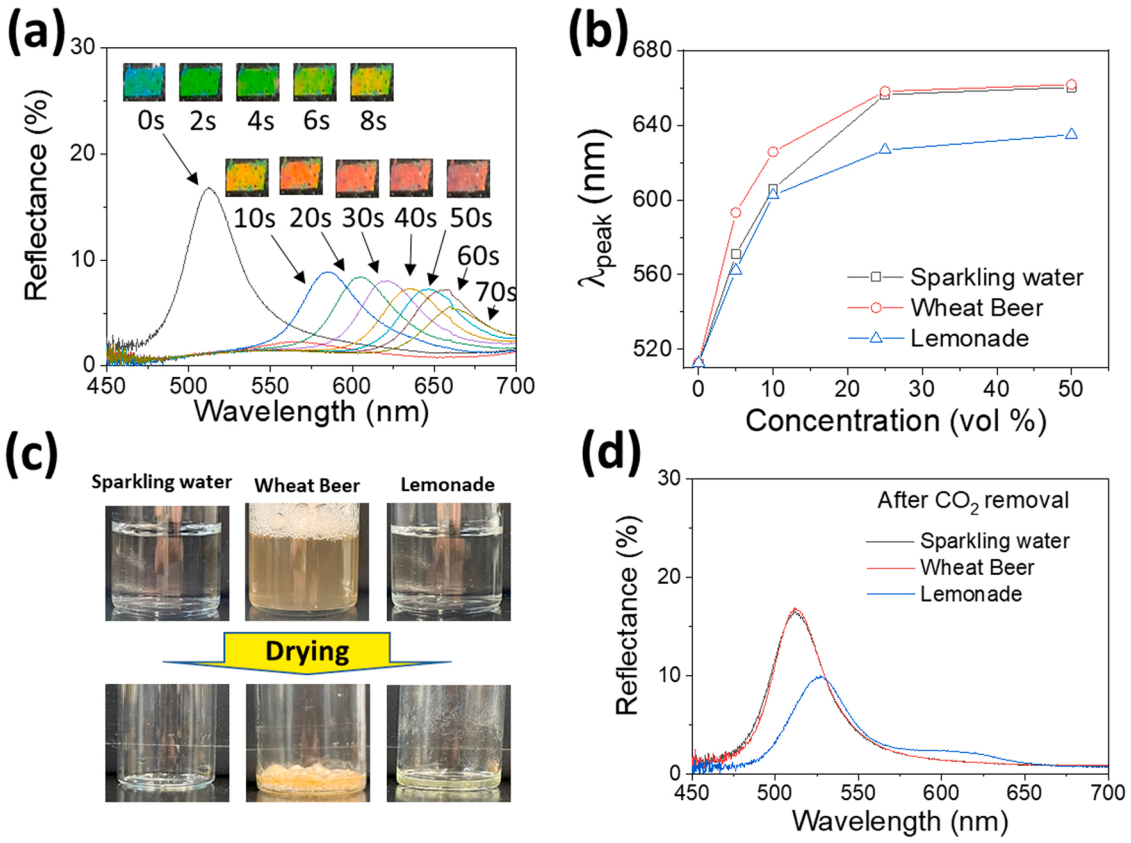

Fig. 7. (a) The time-dependent reflectance spectra and inset photographs of the DMAEMA-IOPG upon contact with sparkling water. (b) The plots of λ_{peak} vs. concentration of three carbonated drinks (sparkling water, wheat beer, and lemonade). (c) Photographic images of the three carbonated drinks before and after drying. (d) The reflectance spectra of the DMAEMA-IOPG in each of the three carbonated drinks after CO_2 removal.

$$CO2(aq) + H2O \leftrightarrow HCO3- + H + K = \frac{[H^+][CO_3^-]}{[CO_2(aq)]} = 4.25 \times 10\text{–}7$$

where $[H^+]$, $[CO_3^-]$, and $[CO_2(aq)]$ are the concentrations of the various components, and K is the equilibrium constant. Here, $[CO_2(aq)]$ can be calculated from the Henry's law constant (K_H) of CO_2, which is ~29.4 atm·L/mol at 25 °C.[35] Thus, if the partial pressure of CO_2 is 0.4 atm, then $[CO_2(aq)]$ is 0.015 M, and the pH is calculated to be 4.1. Under ambient conditions, the time-dependent pH changes of the DI water (3 mL) when supplied with various concentrations of CO_2 (4%, 20%, and 40%) at a total gas flow rate of 25 mL/min are shown in Fig. 6 (b). Thus, with 40% CO_2 supply, the pH of the DI water is seen to gradually decrease from an initial value of 6 to a value of 4.4, which roughly coincides with the calculated pH value of dissolved carbonic acid, at 100 min. The gradual nature of the observed decrease can be attributed to the absence of agitation. Nonetheless, the $\Delta\lambda_{peak}$ owing to pH-driven swelling of pDMAEMA-IOPG will be added to the CO_2 sensor response.

The temperature-dependence of the pDMAEMA-IOPG CO_2 sensing response is shown in Fig. 6(c). The reflectance spectra of the pDMAEMA-IOPG under an N_2 supply at various temperatures are presented in Fig. S7b, and a plot of λ_{peak} vs. temperature is given in Fig. 5(c). Here, there is negligible change in λ_{peak} at room temperature, although a slight decrease is observed in the temperature range of 30–40 °C due to the lower critical solution temperature (LCST) of pDMAEMA at 32 °C,. The time-dependent plots of λ_{peak} measured at 20, 30, 40, and 50 °C in Fig. S8 demonstrate an increased CO_2 response with decreased temperature due to the temperature-dependent solubility of CO_2 gas governed by Henry's law. For this reason, the CO_2 sensing cell was thermostated at 19 ± 1 °C during the experiments, and the measured cell temperatures are shown in Fig. 6(d).

Although the pDMAEMA-IOPGs exhibit fairly good reproducibility and selectivity for CO_2 sensing, the response times are slow by as much as several minutes, especially during CO_2 removal. Although the ascending response time can be reduced to several seconds by bubbling CO_2 gas instead of allowing it to flow over the water surface, the descending response time is not significantly improved by N_2 bubbling. By contrast, a flow of ammonia vapor allows an instantaneous return of λ_{peak} to its initial value during repeated CO_2/NH_3 cycles, thereby providing excellent reproducibility for colorimetric CO_2 sensing, with standard deviation less than 4% (Fig. S9). Thus, the use of ammonia vapor is advantageous for a CO_2 sensor system where a rapid color recovery is required.

As an intriguing application of the colorimetric CO_2 sensor, the color changes of the pDMAEMA-IOPG upon contact with commercial carbonated drinks (sparkling water, wheat ale beer, and lemonade) are investigated in Fig. 7.

As shown in Fig. 7(a), the initial blue-green color of the pDMAEMA-IOPG changes to red within 30 s when the sensor is transferred from DI water to the sparkling water, which had been diluted 4 times. The full RGB color change is observed in the diluted solution because the sparkling water is saturated with CO_2. When the λ_{peak} values are plotted for the pDMAEMA-IOPG in contact with various dilutions of the three carbonated drinks in Fig. 7(b), similar IOPG swelling behaviors are evidenced in the presence of low concentrations of the sparkling water and lemonade, but the IOPG becomes less swollen in the presence of a high concentration of lemonade (>25%) than in high concentrations of the other drinks. Such small variations can be attributed to the differences in ionic species in each drink which can affect the swelling degree of pDMAEMA-IOPG at varying concentration regime.[20] However, the trend in the order of the λ_{peak} values for three carbonated drinks (Beer ~ sparkling water > lemonade) didn't change, implying the order of CO_2

Table 1
The measured amounts of non-volatile solutes and the pH values of the three drinks before and after CO_2 removal.

	Non-volatile solutes (%)	pH (as opened)	pH (CO_2 removed)
Sparkling water	0.7	3.8	6.5
Beer	11.5	4.0	4.3
Lemonade	3.0	3.0	3.2

content. It is reported that typical CO_2 contents in carbonated drinks are ~2.5 vol for beer, 3–5 vol for sparkling water, and 2–3 vol for lemonade, in which 1 vol of CO_2 implies 2 g of CO_2 in 1 L of drink.[36] In contrast to the sparkling water, the beer and lemonade contain dissolved solids such as sugar and spices. When the same volume (10 mL) of each drink is dried in a vacuum oven for 24 h as shown in Fig. 7(c), and the obtained solids are dissolved in DI water (10 mL), the reflectance spectra of the DMAEMA-IOPG in contact with the dissolved solids are as shown in Fig. 7(d). Here, the λ_{peak} values in the CO_2-free sparkling water and beer are the same as that in DI water, in spite of the different amounts of solids in each (Fig. 7d, Table 1) while a red shift of ~20 nm is observed for the CO_2-free lemonade. This result can be attributed to pH-driven swelling of the IOPG in response to the citric acid in the lemonade, which was added by the manufacturer to enhance the citrous flavor. Nevertheless, the λ_{peak} value was still much lower than that in a 10-fold diluted carbonated drink as shown in Fig. 7(b). Thus, it was confirmed that the DMAEMA-IOPG can be utilized for sensing CO_2 concentration in the carbonated drinks.

4. Conclusions

The present study has rigorously investigated the CO_2 response of an inverse opal photonic gel (IOPG) containing dimethyl amino functional groups from the practical point of view. The IOPG based on the monomer 2-(dimethylamino)ethyl methacrylate (DMAEMA) (designated the pDMAEMA-IOPG) showed a better CO_2 responsivity and faster kinetics than sensors based on 2-(dimethylamino)propyl methacrylamide (DMAPMAm). When subjected to repeated cycles of CO_2 and N_2 at a constant total gas flow rate, the color of the optimized pDMAEMA-IOPG sensor changed from green to red as the CO_2 concentration was varied from zero to 100%, with excellent reproducibility over a wide range of CO_2 concentrations. Although pDMAEMA exhibited pH-driven swelling and lower critical solution temperature (LCST) behavior at around 40 °C, the effects of pH and temperature upon the CO_2 response of the IOPG were largely negligible within the experimental conditions. As the pDMAEMA-IOPG responds to carbonate anions, its responses to three commercial carbonated drinks were compared, and the results confirmed the usefulness of the as-developed colorimetric CO_2 sensor.

Declaration of Competing Interest

The authors declare that they have no known competing financial interests or personal relationships that could have appeared to influence the work reported in this paper.

Data availability

Data will be made available on request.

Acknowledgments

The current study was financially supported by the Basic Science Research Program through the National Research Foundation of Korea (NRF), which was funded by the Ministry of Science, ICT, and Future Planning (Grant No. NRF-2019R1A2C1010088), and partially supported by the Institute of Civil Military Technology Cooperation funded by the Defense Acquisition Program Administration and Ministry of Trade, Industry and Energy of Korean government under grant No. 22-CM-C0–01.

Appendix A. Supporting information

Supplementary data associated with this article can be found in the online version at doi:10.1016/j.snb.2022.133041.

References

[1] X. Liu, S.T. Cheng, H. Liu, S. Hu, D.Q. Zhang, H.S. Ning, A survey on gas sensing technology, Sensors 12 (2012) 9635–9665.
[2] K. Potje-Kamloth, Semiconductor junction gas sensors, Chem. Rev. 108 (2008) 367–399.
[3] J.R. Stetter, J. Li, Amperometric gas sensors - a review, Chem. Rev. 108 (2008) 352–366.
[4] H.A. Haugen, L.-N. Chan, F. Li, Indirect calorimetry: a practical guide for clinicians, Nutr. Clin. Pr. 22 (2007) 377–388.
[5] P. Puligundla, J. Jung, S. Ko, Carbon dioxide sensors for intelligent food packaging applications, Food Control 25 (2012) 328–333.
[6] G. Duxbury, N. Langford, M.T. McCulloch, S. Wright, Quantum cascade semiconductor infrared and far-infrared lasers: from trace gas sensing to non-linear optics, Chem. Soc. Rev. 34 (2005) 921–934.
[7] T.A. Vincent, J.W. Gardner, A low cost MEMS based NDIR system for the monitoring of carbon dioxide in breath analysis at ppm levels, Sens. Actuators B 236 (2016) 954–964.
[8] T. Lang, H.D. Wiemhofer, W. Gopel, Carbonate based CO_2 sensors with high performance, Sens. Actuators B 34 (1996) 383–387.
[9] M. Struzik, I. Garbayo, R. Pfenninger, J.L.M. Rupp, A simple and fast electrochemical CO_2 sensor based on Li7La3Zr2O12 for environmental monitoring, Adv. Mater. 30 (2018), 184098.
[10] M. Uttamlal, D.R. Walt, A. Fiber-Optic, Carbon dioxide sensor for fermentation monitoring, Nat. Biotech. 13 (1995) 597–601.
[11] V.L. Alexeev, A.C. Sharma, A.V. Goponenko, S. Das, I.K. Lednev, C.S. Wilcox, et al., High ionic strength glucose-sensing photonic crystal, Anal. Chem. 75 (2003) 2316–2323.
[12] S.A. Asher, A.C. Sharma, A.V. Goponenko, M.M. Ward, Photonic crystal aqueous metal cation sensing materials, Anal. Chem. 75 (2003) 1676–1683.
[13] J.-P. Couturier, M. Sutterlin, A. Laschewsky, C. Hettrich, E. Wischerhoff, Responsive inverse opal hydrogels for the sensing of macromolecules, Angew. Chem. Int. Ed. 54 (2015) 6641–6644.
[14] M. Gallei, Functional polymer opals and porous materials by shear-induced assembly of tailor-made particles, Macromol. Rapid Com. 39 (2018) 1700648.
[15] W. Hong, Y. Chen, X. Feng, Y. Yan, X.B. Hu, B.Y. Zhao, et al., Full-color CO_2 gas sensing by an inverse opal photonic hydrogel, Chem. Comm. 49 (2013) 8229–8231.
[16] K. Lee, S.A. Asher, Photonic crystal chemical sensors: pH and ionic strength, J. Am. Chem. Soc. 122 (2000) 9534–9537.
[17] Y.J. Lee, P.V. Braun, Tunable inverse opal hydrogel pH sensors, Adv. Mater. 15 (2003) 563–566.
[18] M. Li, Q. Lyu, B. Peng, X. Chen, L. Zhang, J. Zhu, Bioinspired colloidal photonic composites: fabrications and emerging applications, Adv. Mater. 2110488 (2022) 2110488.
[19] C.G. Schafer, T. Winter, S. Heidt, C. Dietz, T. Ding, J.J. Baumberg, et al., Smart polymer inverse-opal photonic crystal films by melt-shear organization for hybrid core–shell architectures, J. Mater. Chem. C. 3 (2015) 2204–2214.
[20] J. Shin, P.V. Braun, W. Lee, Fast response photonic crystal pH sensor based on templated photo-polymerized hydrogel inverse opal, Sens. Actuators B 150 (2010) 183–190.
[21] W. Wang, Y. Zhou, L. Yang, X. Yang, Y. Yao, Y. Meng, Stimulus-responsive photonic crystals for advanced security, Adv. Func. Mater. 32 (2022) 2204744.
[22] M. Xu, A.V. Goponenko, S.A. Asher, Polymerized polyHEMA photonic crystals: pH and ethanol sensor materials, J. Am. Chem. Soc. 130 (2008) 3113–3119.
[23] B. Kim, K.Y. J, W. Kang, Lee, An anion sensing photonic gel by hydrogen bonding of anions to the N-allyl-N′-ethyl urea receptor, J. Mater. Chem. A 2 (2014) 5682–5687.
[24] S.A. Asher, K.W. Kimble, J.P. Walker, Enabling thermoreversible physically cross-linked polymerized colloidal array photonic crystals, Chem. Mater. 20 (2008) 7501–7509.
[25] J.H. Kang, J.H. Moon, S.K. Lee, S.G. Park, S.G. Jang, S. Yang, et al., Thermoresponsive hydrogel photonic crystals by three-dimensional holographic lithography, Adv. Mater. 20 (2008) 3061–3065.
[26] Y. Takeoka, M. Watanabe, Tuning structural color changes of porous thermosensitive gels through quantitative adjustment of the cross-linker in pre-gel solutions, Langmuir 19 (2003) 9104–9106.
[27] R.A. Barry, P. Wiltzius, Humidity-Sensing Inverse Opal Hydrogels, Langmuir 22 (2006) 1369–1374.
[28] O. Garcia-Valdez, T. Brescacin, J. Arredondo, J. Bouchard, P.G. Jessop, P. Champagne, et al., Grafting CO_2-responsive polymers from cellulose nanocrystals via nitroxide-mediated polymerisation, Polym. Chem. -Uk 8 (2017) 4124–4131.

[29] S.-G. Kim, Y.-G. Seo, Y.-J. Cho, J.-S. Shin, S.-C. Gil, W.-M. Lee, Optimization of emulsion polymerization for submicron-sized polymer colloids towards tunable synthetic opals, Bul. Kor Chem. Soc. 31 (2010) 1891–1896.
[30] S. Lee, Y.-L. Lee, B. Kim, K. Kwon, J. Park, K. Han, et al., Rapid on-chip integration of opal films and photonic gel sensor array via directed enhanced water evaporation for colloidal assembly, Sens. Actuators B 231 (2016) 256–264.
[31] M.D. Hanwell, D.E. Curtis, D.C. Lonie, T. Vandermeersch, E. Zurek, G. R. Hutchinson, Avogadro: an advanced semantic chemical editor, visualization, and analysis platform, J. Chemin.-. 4 (2012) 17.
[32] J. Shin, S.G. Han, W. Lee, Inverse opal pH sensors with various protic monomers copolymerized with polyhydroxyethylmethacrylate hydrogel, Anal. Chim. Act. 752 (2012) 87.
[33] R.B. Said, J.M. Kolle, K. Essalah, B. Tangour, A. Syari, A unified approach to CO_2−amine reaction mechanisms, ACS Omega 5 (2020) 26125–26133.
[34] F. Liu, W. Fu, S. Chen, Synthesis, characterization and CO_2 adsorption performance of a thermosensitive solid amine adsorbent, J. CO_2 Util. 31 (2019) 98–105.
[35] D.D. Miller, S.S.C. Chuang, Control of CO_2 adsorption and desorption using polyethylene glycol in a tetraethylenepentamine thin film: an in situ ATR and theoretical study, J. Phys. Chem. C. 120 (2016) 25489–25504.
[36] R. Sanders, W.E. Acree, A.D. Visscher, S.E. Schwartz, T.J. Wallington, Henry's law constants, Pure Appl. Chem. 94 (2022) 71–85.

Nam Yeon Heo is a graduate student of the Department of Chemistry at Sejong University. He received BS degree from Sejong University in 2018 at the Department of Chemistry. His expertise is on the synthesis and application of opal photonic crystals, colorimetric sensors.

Donghoon Kim is a graduate student of the Department of Chemistry at Sejong University. He received BS degree from Sejong University in 2020 at the Department of Chemistry. His expertise is on the synthesis and application of various hydrogels, colloidal self-assembly, and inverse opal sensors.

Shin Geun Park is a graduate student of the Department of Chemistry at Sejong University. He received BS degree from Gunsan University in 2020 at the Department of Chemistry. His expertise is on the synthesis and application of metal oxide nanoparticles, radical polymerizations, photonic balls, and colloidal self-assembly.

Hyunjung Lee is a Professor of the College of Advanced Materials Engineering at Kookmin University. She received PhD degree in 2001 from Pohang University of Science and Technology, majoring polymer chemistry. After post-doctoral periods in University of Illinois at Urbana-Champaign (UIUC) and Massachusetts Institute of Technology (MIT), Prof. Lee worked at Korea Institute of Science and Technology (KIST) as a senior researcher. She is now a full professor at Kookmin University since 2010. Prof. Lee's research area includes the photonic materials, sensors, and thermoelectric materials and devices.

Wonmok Lee is a Professor of the Department of Chemistry at Sejong University. He received his PhD degree in 2001 from Pohang University of Science and Technology, majoring polymer chemistry. After post-doctoral periods in University of Illinois at Urbana-Champaign (UIUC) and Massachusetts Institute of Technology (MIT), Prof. Lee developed an industrial career at Samsung Advanced Institute of Technology (SAIT). He is now a full professor at Sejong University since 2007. Prof. Lee's research area covers the colloids, sensors, displays, and sustainable energy devices.